

# Persistent Homology Reveals the Role of Stiffness in Forming Topological Glasses in Dense Solutions of Ring Polymers

Shota Goto,<sup>†</sup> Takenobu Nakamura,<sup>‡</sup> Davide Michieletto,<sup>¶,§</sup> Kang Kim,<sup>\*,†</sup> and Nobuyuki Matubayasi<sup>\*,†</sup>

<sup>†</sup>*Division of Chemical Engineering, Department of Materials Engineering Science, Graduate School of Engineering Science, Osaka University, Toyonaka, Osaka 560-8531, Japan*

<sup>‡</sup>*National Institute of Advanced Industrial Science and Technology (AIST), 1-1-1 Umezono, Tsukuba, Ibaraki 305-8568, Japan*

<sup>¶</sup>*School of Physics and Astronomy, University of Edinburgh, Peter Guthrie Tait Road, Edinburgh, EH9 3FD, UK*

<sup>§</sup>*MRC Human Genetics Unit, Institute of Genetics and Cancer, University of Edinburgh, Edinburgh, EH4 2XU, UK*

E-mail: [kk@cheng.es.osaka-u.ac.jp](mailto:kk@cheng.es.osaka-u.ac.jp); [nobuyuki@cheng.es.osaka-u.ac.jp](mailto:nobuyuki@cheng.es.osaka-u.ac.jp)

## Abstract

Ring polymers are characterized by topology-specific entanglements called threadings. In the limit of large rings, it is conjectured that a “topological glass” should emerge due to the proliferation of threadings. In this study, we used persistent homology to quantify threading structures of ring polymers with different chain stiffness and elucidate mechanisms behind topological glasses. Using coordination data from

coarse-grained molecular dynamics simulations, we analyzed the topology of the union of virtual spheres centered on each monomer or center of mass. As the radius of each sphere increases, the corresponding points connect, giving rise to topological entities such as edges, loops, and facets. We then analyzed how the number of loops per ring chain and penetrated loops varies with sphere radius, focusing on the effects of chain stiffness and density. The results reveal that loops are larger in stiff ring chains, whereas flexible ring chains do not generate sufficiently large loops to establish a threading structure. The stiffness of ring polymer plays a significant role in the formation of topological glasses in ring polymers.

Ring polymers exhibit distinctive properties compared to their linear counterparts.<sup>1-4</sup> Despite extensive research, a thorough understanding of topological constraints in ring polymer melts remains a significant challenge in polymer physics.<sup>5-29</sup> One key feature thought to define topological constraints in ring polymers is the interpenetrating structure known as “threading”. Threading occurs when one ring polymer penetrates the loop of another ring polymer, with the penetrating ring classified as active and the penetrated ring as passive, illustrating the asymmetric and hierarchical nature of the threading network. For sufficiently long rings, this threading network can evolve, eventually leading to the formation of “topological glasses,” where the relaxation time is expected to increase drastically with respect to the extent of threading.<sup>30-33</sup>

Analyzing threading and clarifying its relationship with glass-like properties is crucial. While several approaches for quantifying threading have been proposed, including methods based on minimal surface<sup>34,35</sup> and geometric analysis,<sup>36,37</sup> Landuzzi et al. introduced a method for quantifying the threading of ring polymers using persistent homology (PH).<sup>38</sup> PH is a mathematical tool that characterizes topological features such as “loops” from point cloud.<sup>39-41</sup> Specifically, Landuzzi et al. investigated threading structures using PH from MD simulations with the Kremer–Grest (KG) model<sup>42</sup> for ring polymers. Of particular interest was the chain length  $N$  dependence of ring polymers up to  $N = 2048$  at a monomer

number density of 0.1, incorporating a bending potential  $U_{\text{bend}}(\theta) = \varepsilon_{\theta}(1 + \cos \theta)$ , where  $\theta$  represents the angle formed by consecutive bonds and  $\varepsilon_{\theta} = 5$  (see Eq. (3) for details). This bending potential effectively models the polymers as worm-like chains, analogous to the Kratky–Porod model.<sup>43</sup>

We recently performed MD simulations using the KG with two types of ring polymers: semi-flexible ( $\varepsilon_{\theta} = 1.5$ ) and stiff ( $\varepsilon_{\theta} = 5$ ) rings with a fixed chain length  $N = 400$  to investigate the influence of chain stiffness on their dynamic properties.<sup>44</sup> The rearrangement dynamics of the center of mass (COM) were analyzed, with a focus on dynamic heterogeneity to clarify glassy behavior. Our results demonstrated that stiff ring polymers exhibit pronounced glassy behavior accompanied by dynamic heterogeneity, whereas semi-flexible ring polymers display homogeneous dynamics characterized by a Gaussian distribution of COM displacement. This distinction suggests that the dynamic properties of ring polymers are fundamentally influenced by the chain stiffness, emphasizing the need to examine threading structures across varying degrees of chain stiffness.

The purpose of this study is to elucidate the influence of the chain stiffness and monomer number density of ring polymers on their threading structures. We first analyze the connectivity of COM using PH. Subsequently, we characterize the active and passive threading structures between pairs of ring chains through PH. Through these analyses, we clarify the topological characteristics of ring polymers and their relationship to glassy behavior, informed by insights gained from the rearrangement dynamics of COM.

### **Model and Methodology**

We employed MD simulations for ring polymer dense solutions utilizing the KG model. Each ring polymer is represented by  $N$  monomer beads, each with mass  $m$  and diameter  $\sigma$ . The system comprises  $M$  ring chains contained within a three-dimensional cubic box with volume of  $V$ , with periodic boundary conditions. The monomer beads interact through three types of inter-particle potentials: the Lennard-Jones (LJ) potential governs the interaction between

all pairs of monomer beads and is defined as

$$U_{\text{LJ}}(r) = 4\varepsilon_{\text{LJ}} \left[ \left( \frac{\sigma}{r} \right)^{12} - \left( \frac{\sigma}{r} \right)^6 \right] + C, \quad (1)$$

where  $r$  is the distance between two beads,  $\varepsilon_{\text{LJ}}$  is the depth of the potential well, and  $C$  is a constant that shifts the potential at the cut-off distance of  $r_c = 2^{1/6} \sigma$ . Two adjacent monomer beads along the chain also interacted via the finitely extensible nonlinear elastic (FENE) bond potential

$$U_{\text{LENE}}(r) = -\frac{1}{2}KR_0^2 \ln \left[ 1 - \left( \frac{r}{R_0} \right)^2 \right], \quad (2)$$

for  $r < R_0$ , where  $K$  and  $R_0$  represent the spring constant and the maximum length of the bond, respectively. We used the values of  $K = 30\varepsilon_{\text{LJ}}/\sigma^2$  and  $R_0 = 1.5\sigma$ . Lastly, the chain stiffness is controlled by incorporating a bending potential

$$U_{\text{bend}}(\theta) = \varepsilon_\theta [1 - \cos(\theta - \theta_0)], \quad (3)$$

where  $\theta$  is the bending angle formed by three consecutive monomer beads along the polymer chain. In this study, the bending energy was set as  $\varepsilon_\theta/\varepsilon_{\text{LJ}} = 0, 1.5, 2, 3, 4,$  and  $5$ , with an equilibrium angle of  $\theta_0 = 180^\circ$ .

All MD simulations were performed using the Large-scale Atomic/Molecular Massively Parallel Simulator (LAMMPS).<sup>45</sup> Length, energy and time are represented in units of  $\sigma$ ,  $\varepsilon_\theta$  and  $(m/\varepsilon_{\text{LJ}})^{1/2}$ , respectively. Additionally, the temperature is expressed in units of  $\varepsilon_{\text{LJ}}/k_{\text{B}}$ , where  $k_{\text{B}}$  is Boltzmann constant. We fixed the temperature  $T$ , chain length  $N$ , number of chains  $M$  as  $T = 1.0$  and  $N = 400$ , and  $M = 100$ , respectively. Throughout the simulations, temperature was controlled using the Nosé–Hoover thermostat, with a time step of  $\Delta t = 0.01$ . The monomer number density  $\rho\sigma^3$  ( $= NM\sigma^3/V$ ) was varied as  $0.1, 0.2, 0.3, 0.4,$  and  $0.5$  for each degree of chain stiffness. Henceforth,  $\rho$  will be referred to as density.

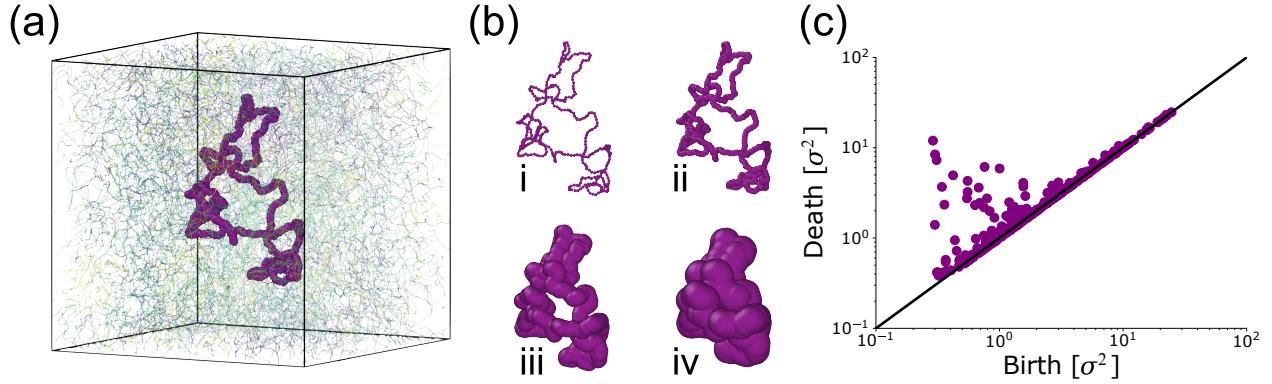


Figure 1: Persistent diagram of a ring polymer with chain length  $N = 400$  at density  $\rho = 0.1$ . (a) Snapshot of entangled ring polymer chains. (b) Virtual spheres with radii  $\sqrt{\alpha}$  assigned on each monomer bead of an arbitrary ring. (c) Persistent diagram of the ring.

Here, we briefly outline PH: A set of coordinates such as beads of chains or COM, denoted as  $\{\mathbf{r}\} = \{\mathbf{r}_1, \mathbf{r}_2, \dots, \mathbf{r}_\kappa\}$ , is used as input data, where  $\kappa$  is the number of coordinates. At each coordinate, assign a virtual sphere with radius  $\sqrt{\alpha}$ , where  $\alpha$  is a parameter. Initially, when  $\alpha = 0$ , all points are treated as disconnected components. As  $\alpha$  increases, the spheres begin to overlap, and connected components form, creating edges and facets. During this process, the topological features varies discontinuously with respect to  $\alpha$ , *i.e.*, the loops will appear and disappear. We record the radii for appearance and disappearance as  $b$  (birth) and  $d$  (death) respectively for each hole, and introduce persistence diagram (PD) as a collection  $(b, d)$  of all holes. In this context, a zero-dimensional hole represents a connected component, while a one-dimensional hole represents a loop. The instance of the PH procedure is illustrated in Fig. 1, which shows the PD of a ring polymer in solution.

PD captures not only the topological features at a specific radius, *i.e.*, a threshold of connection, but also how these features change as the threshold increases. All analysis were performed using the HomCloud.<sup>46</sup>

### Connectivity of Centers of Mass in Ring Polymer Solutions

The first analysis aims to reveal the connectivity of the COM coordinates of ring polymer chains using PH. The number of connected components at a given  $\alpha$ , denoted as  $\beta_0(\alpha)$  and referred to as the zero-th Betti number, is calculated. As the radius of the virtual sphere

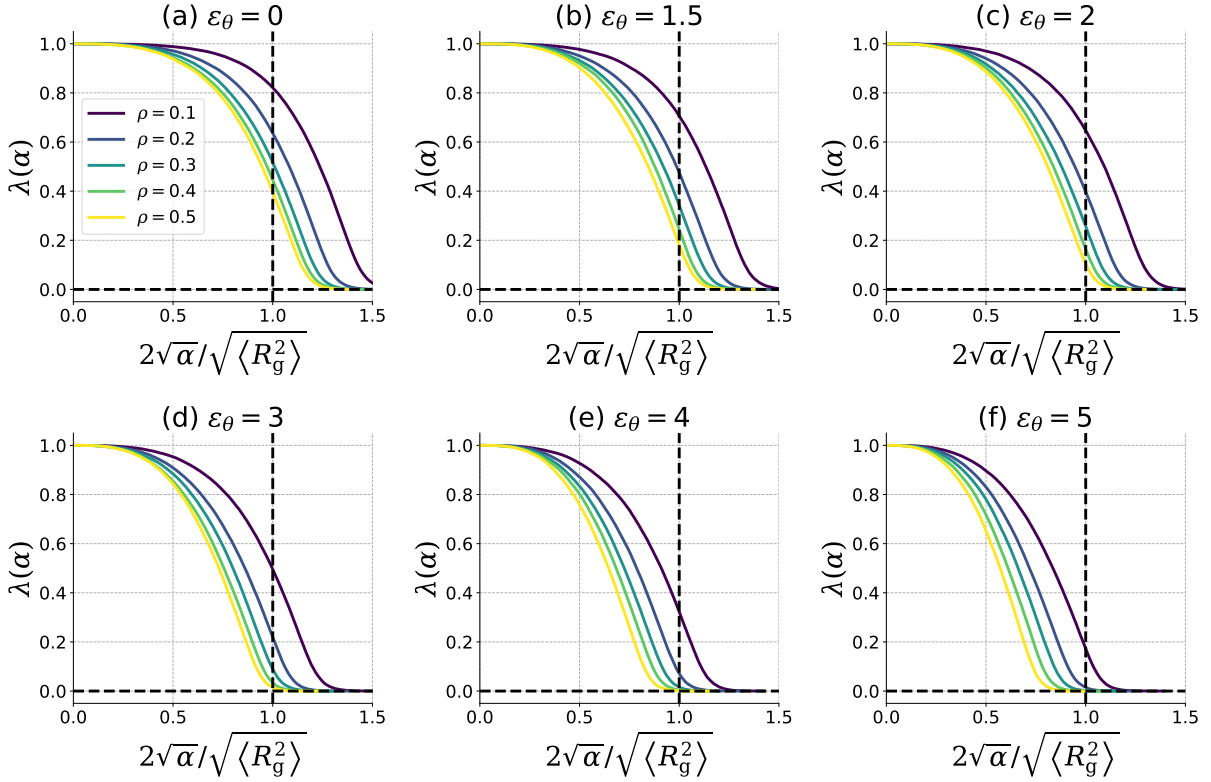


Figure 2: Density  $\rho$  dependence of  $\lambda(\alpha)$  as a function of  $2\sqrt{\alpha}/\sqrt{\langle R_g^2 \rangle}$  by varying the bending energy  $\varepsilon_\theta = 0$  (a),  $\varepsilon_\theta = 1.5$  (b),  $\varepsilon_\theta = 2$  (c),  $\varepsilon_\theta = 3$  (d),  $\varepsilon_\theta = 4$  (e), and  $\varepsilon_\theta = 5$  (f). The horizontal and vertical dashed lines represent  $\lambda = 0$  and  $\alpha = \langle R_g^2 \rangle / 2$ , respectively.

with a radius of  $\sqrt{\alpha}$  expands, spheres will connect each other and finally become one lump. Thus,  $\beta_0(\alpha)$  converges to unity as  $\alpha$  approaches infinity. We define the function representing the decrease in  $\beta_0(\alpha)$  as

$$\lambda(\alpha) = \left\langle \frac{\beta_0(\alpha) - 1}{\beta_0(0) - 1} \right\rangle, \quad (4)$$

where  $\langle \dots \rangle$  represents the statistical average over the snapshot configurations generated by MD simulations; note that  $\beta_0(\alpha)$  can be determined for each snapshot. Accordingly, this function takes the value  $\lambda(\alpha = 0) = 1$  and  $\lambda(\alpha \rightarrow \infty) = 0$ . The density  $\rho$  dependence of  $\lambda(\alpha)$  is plotted in Fig. 2 by varying the bending energy  $\varepsilon_\theta$ . In the plot, the horizontal axis is represented by  $2\sqrt{\alpha}/\sqrt{\langle R_g^2 \rangle}$  with the mean square gyration of radius  $\langle R_g^2 \rangle$  of the ring chains. Note that the COM distance between any pair of two ring polymers,  $i$  and  $j$ , is related as

$r_{ij} = 2\sqrt{\alpha}$  when the rings are in contact, since the radius of the sphere in the PH analysis is  $\sqrt{\alpha}$ .

Figure 2 demonstrates that  $\lambda(\alpha)$  decreases and converges to zero at a specific length scale  $\alpha$ . This behavior indicates percolation, where clusters are formed by virtually connected COMs. The characteristic length scale is  $\alpha = \langle R_g^2 \rangle / 2$ , where a virtual bond is considered to have formed if the distance  $r_{ij}$  between the COMs of ring polymer pair  $(i, j)$  satisfies  $r_{ij} \leq \langle R_g^2 \rangle$  (see horizontal lines in Fig. 2). For flexible ring chains with  $\varepsilon_\theta = 0$ ,  $\lambda$  takes finite values for  $\alpha \leq \langle R_g^2 \rangle$  across all densities, indicating the presence of numerous small clusters. In contrast, stiff ring chains with  $\varepsilon_\theta = 5$  exhibit  $\lambda \approx 0$  at  $\alpha = \langle R_g^2 \rangle / 2$ , suggesting the formation of percolated networks among COMs of ring chains. Furthermore, the length scale of  $\alpha$  exhibiting a plateau of  $\lambda \approx 1$  approximately corresponds to the characteristic core length, analogous to the behavior of ring polymers modeled as soft macromolecules. As  $\varepsilon_\theta$  increases, this core length is reduced, as shown in Fig. 2. These findings indicate that in flexible ring chains, the cores are large and overlap each other, but their COMs are not connected with one another. In contrast, for stiff ring chains, the smaller cores and relatively larger radius of gyration lead to an increase in the number of virtual bonds between COMs. Thus, the density and chain stiffness strongly influence the structural and dynamic behavior of ring polymer systems. See Supporting Information for further discussion on the dependence on chain stiffness and density dependence of the mean square gyration of radius  $\langle R_g^2 \rangle$ , radial distribution function of COMs,  $g(r)$ , and the number of virtual bonds  $Z_b$  defined by the radial distribution function of COMs, as shown in Fig. S1-S3 in Supporting Information, respectively.

The next analysis focuses on the one-dimensional hole, *i.e.* “loop” structure, characterized by PH. Specifically, PH is performed on each individual ring polymer  $i$  by using the monomer coordinates as input, which generates a persistent diagram (PD) denoted as  $\text{PD}(i)$ . This analysis reveals the birth and death of topological features such as loops within the structure of the polymer. Furthermore, the “life” of the loop is defined as the vertical distance from

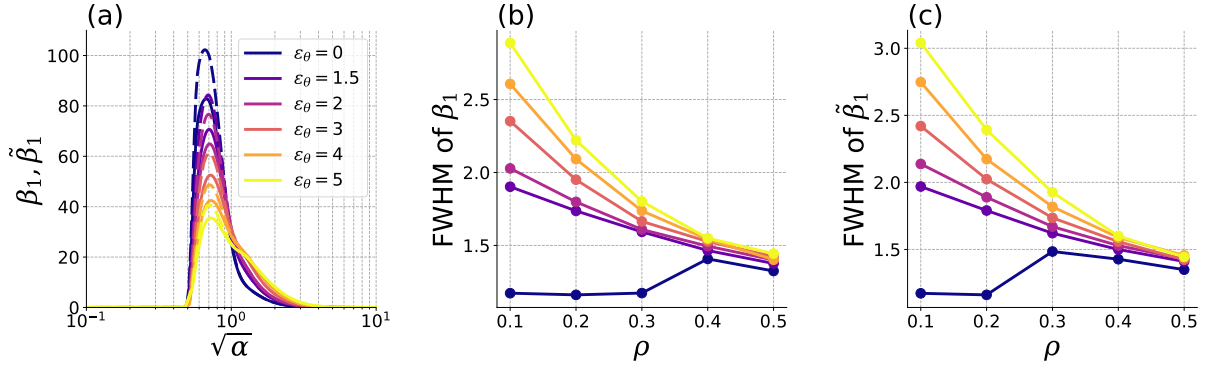


Figure 3: (a) Chain stiffness  $\varepsilon_\theta$  dependence of  $\beta_1(\alpha)$  and  $\tilde{\beta}_1(\alpha)$  at the highest density  $\rho = 0.5$ . (b), (c) Plots of full width at half maximum (FWHM) of  $\beta_1(\alpha)$  and  $\tilde{\beta}_1(\alpha)$  as a function of density  $\rho$ , respectively.

the diagonal line in the PD, denoted as  $l = d - b$ , which quantifies how long during the increase of  $\alpha$  the loop persists before disappearing. Thus, larger values of  $l$  indicates longer-lived loops, reflecting more stable topological features of the system against the change of threshold. Next, we performed PH for  $(i, j)$  pairs of ring polymer chains using the set of their coordinates as input, generating PD denoted as  $\text{PD}(i \cup j)$ . Since threading occurs when the loop of one ring polymer disappears due to penetration by another polymer,  $\text{PD}(j \rightarrow i) = \text{PD}(i) \setminus \text{PD}(i \cup j)$  allows us to quantify the loops being threaded.<sup>38</sup> Here, the set difference operator  $\setminus$  represents the subtraction of topological features that vanish when polymer  $j$  interacts with polymer  $i$ . In this context, polymer  $i$  is considered “passive” while polymer  $j$  is the “active” participant in the threading process. Thus, this approach quantifies the threading structures between pairs of ring polymers. The probability density distributions of  $\text{PD}(i)$ ,  $\text{PD}(i \cup j)$ , and  $\text{PD}(j \rightarrow i)$  with  $\varepsilon_\theta = 1.5$  and 5 at densities  $\rho = 0.1$  and 0.5 are shown in Fig. S4-S7 in Supporting Information.

### Chain Stiffness Effects on Loops and Threading in Ring Polymers

To analyze the threading structure by varying the density  $\rho$  and chain stiffness  $\varepsilon_\theta$ , we quantify



the first Betti number,  $\beta_1^{(i)}(\alpha)$ , in the PD( $i$ ). This is defined by

$$\beta_1^{(i)}(\alpha) = \int_{\alpha}^{\infty} dd \int_0^{\infty} db \sum_k \delta(b - b_k^{(i)}) \delta(d - d_k^{(i)}), \quad (5)$$

where  $k$  refers to the  $k$ -th loop on the ring chain  $i$ . This  $\beta_1(\alpha)$  quantifies the number of loops in the region where  $b < \alpha$  and  $d > \alpha$ , quantifying the number of loops observed at a given  $\alpha$ . The average of  $\beta_1^{(i)}(\alpha)$  over all ring chains can be expressed as

$$\beta_1(\alpha) = \left\langle \frac{1}{N} \sum_i \beta_1^{(i)}(\alpha) \right\rangle. \quad (6)$$

The same calculation can be performed for PD( $j \rightarrow i$ ), and the average over all pairs of ring chains ( $i, j$ ) are denoted as  $\tilde{\beta}_1(\alpha)$ . This  $\tilde{\beta}_1(\alpha)$  measures the number of loops that are being threaded by other ring chains. Consequently, it is assured that  $\beta_1(\alpha) \geq \tilde{\beta}_1(\alpha)$ . Furthermore,  $\beta_1(\alpha)$  and  $\tilde{\beta}_1(\alpha)$  converges asymptotically to zero with respect to each other as  $\alpha$  becomes sufficiently large.

Figure 3(a) shows the density  $\rho$  dependence of  $\beta_1(\alpha)$  and  $\tilde{\beta}_1(\alpha)$  at the highest density  $\rho = 0.5$ . The stiff ring exhibits a broader peak at larger length scales  $\alpha$  compared to that of the flexible ring, indicating the presence of large loops. Peaks emerge and decay over similar length scales for both  $\beta_1(\alpha)$  and  $\tilde{\beta}_1(\alpha)$ . The peak intensity, however, depends on the chain stiffness  $\varepsilon_{\theta}$ . For sufficiently large  $\alpha$ , the convergence of  $\beta_1 \sim \tilde{\beta}_1$  indicates that all large loops are involved in threading. The all results of  $\beta_1(\alpha)$  and  $\tilde{\beta}_1(\alpha)$  with varying  $\varepsilon_{\theta}$  and  $\rho$  are shown in Fig. S8 in Supporting Information.

The full width at half maximum (FWHM) of  $\beta_1(\alpha)$  and  $\tilde{\beta}_1(\alpha)$  are plotted in Fig. 3(b) and (c). Note that the FWHM provides insights into average behavior of loop sizes. The FWHM of  $\beta_1(\alpha)$  and  $\tilde{\beta}_1(\alpha)$  are larger for stiff rings compared to those of flexible rings, indicating that stiff rings have a broader distribution of loop sizes at low density. As the density increases, the FWHM of  $\beta_1(\alpha)$  and  $\tilde{\beta}_1(\alpha)$  converge to a common value. This result suggests that the stiffness of ring chains significantly influences the formation of large loops in dilute solutions,

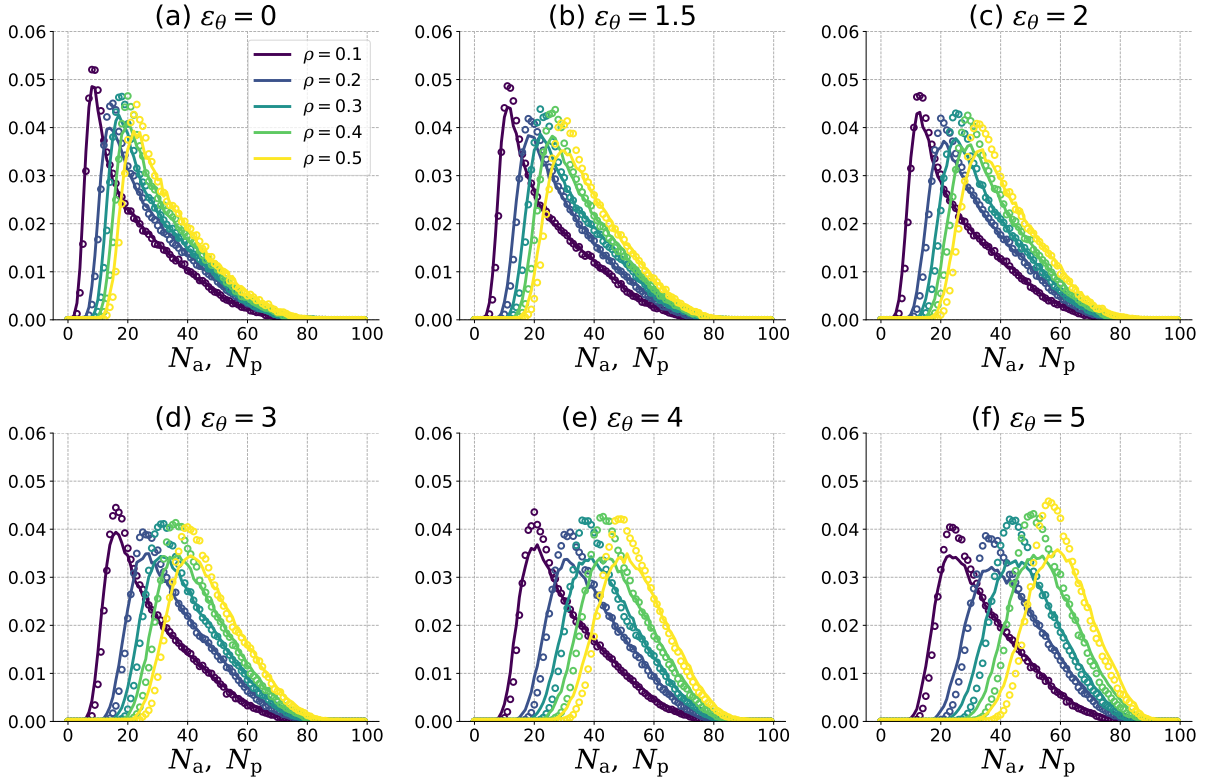


Figure 4: Density  $\rho$  dependence of probability density distribution of active threading number  $N_a$  (points) and passive threading number  $N_p$  (solid curves) by varying the bending energy  $\varepsilon_\theta = 0$  (a),  $\varepsilon_\theta = 1.5$  (b),  $\varepsilon_\theta = 2$  (c),  $\varepsilon_\theta = 3$  (d),  $\varepsilon_\theta = 4$  (e), and  $\varepsilon_\theta = 5$  (f). The threshold value is fixed at  $l_{\text{th}} = 0$ .

while the rings strongly overlap and shrink the size of loops as the density increases. Note that flexible ring chains with  $\varepsilon_\theta = 0$  exhibit non-monotonic behavior at low density  $\rho \leq 0.3$ . This behavior is attributed to the peak of  $\beta_1(\alpha)$  at  $\alpha \approx 0.6$ , as shown in Fig. S8(a), which is resulted from short-lived loops along the diagonal line in the PD.

### Assymetry between Active and Passive Threading

We further examine the active threading number  $N_a$ , which represents the number of rings penetrated by a given ring, and the passive threading number  $N_p$ , which denotes the number

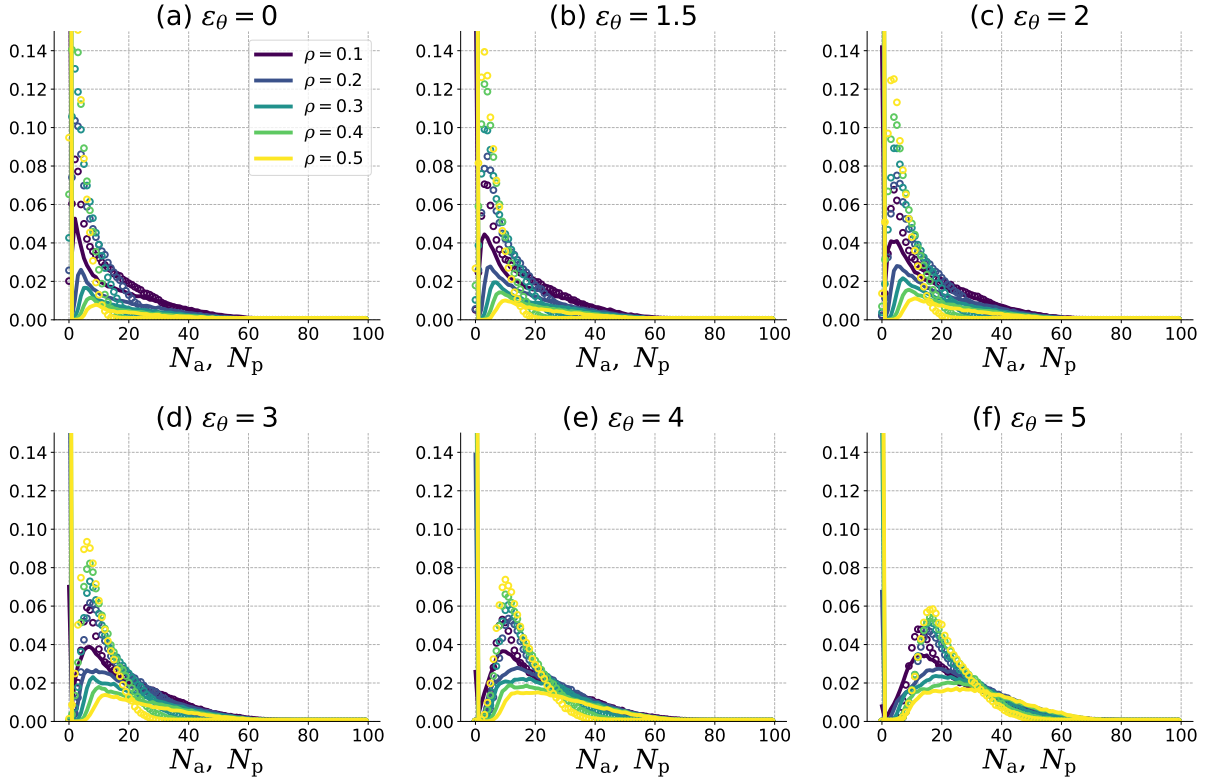


Figure 5: Density  $\rho$  dependence of probability density distribution of active threading number  $N_a$  (points) and passive threading number  $N_p$  (solid curves) by varying the bending energy  $\varepsilon_\theta = 0$  (a),  $\varepsilon_\theta = 1.5$  (b),  $\varepsilon_\theta = 2$  (c),  $\varepsilon_\theta = 3$  (d),  $\varepsilon_\theta = 4$  (e), and  $\varepsilon_\theta = 5$  (f). The threshold value is fixed at  $l_{\text{th}} = 9$ .

of rings that experience penetration by that same ring. For the pair  $(i, j)$ , we define

$$I_{j \rightarrow i}^{(k)} = \begin{cases} 1 & \text{if } l_k \geq l_{\text{th}} \\ 0 & \text{if } l_k < l_{\text{th}} \end{cases} \quad (7)$$

where  $l_k$  represents the life of the  $k$ -th loop in  $\text{PD}(j \rightarrow i)$ , and  $l_{\text{th}}$  is a threshold value for the life used to characterize the length scale of threading. By summing over loop  $k$  and polymer  $j$  ( $i$ ), the active (passive) threading number,  $N_{a,j}$  ( $N_{p,j}$ ) for polymer  $j$  ( $i$ ) are obtained,

expressed as follows:

$$N_{a,j} = \sum_i \sum_k I_{j \rightarrow i}^{(k)}, \quad N_{p,i} = \sum_j \sum_k I_{j \rightarrow i}^{(k)}. \quad (8)$$

Furthermore, the averages over all ring chains are denoted by  $N_a$  and  $N_p$ , respectively. Their statistical averages over all chains ensure  $\langle N_a \rangle = \langle N_p \rangle$  because, when threading occurs, active and passive threading are always counted once, respectively.

Figure 4 presents the probability density distribution of  $N_a$  and  $N_p$ , respectively. Note that  $N_a$  and  $N_p$  were calculated by including threading at all length scales, with the threshold  $l_{\text{th}}$  set to zero. It is demonstrated that for both  $N_a$  and  $N_p$ , the peak shifts to higher values with increasing chain stiffness  $\varepsilon_\theta$  and density  $\rho$ , indicating a greater occurrence of threading. Notably, the density dependence of the distribution becomes more pronounced for stiff rings compared to that of flexible rings. In addition,  $N_p$  exhibits a slightly broader distribution than  $N_a$  at high density for stiff rings. This asymmetric property between  $N_a$  and  $N_p$  was found to be pronounced for longer stiff rings, suggesting that the passive threading is significantly influenced by the presence of long-lived loops. In other words, larger loops are likely to be involved in the passive threading.

We further characterize the long-lived active and passive threading structures by introducing the threshold value  $l_{\text{th}}$ , which has a dimension  $\sigma^2$ . Since points near the diagonal line are considered noisy, we introduce  $l_{\text{th}}$  to filter out threading associated with loops of short life, thereby characterizing loops that are mostly correlated with topological constraints. While the results for varying  $l_{\text{th}}$  are not displayed, the threshold value  $l_{\text{th}} = 9$  was determined to capture the most relevant characteristics, and the corresponding results are shown below.

Figure 5 illustrates the density dependence of probability density distribution of active and passive threading numbers,  $N_a$  and  $N_b$ , at  $l_{\text{th}} = 9$ . For flexible ring chains, both  $N_a$  and  $N_p$  show the tendency of the decrease toward zero as the density  $\rho$  increases. This

trend is expected to become more pronounced as the threshold value  $l_{\text{th}}$  increases. This observation suggests that the number of loops necessary for threading becomes minimal in higher densities, consistent with the overlapping structures between the crumbled globules characteristic of flexible ring chains. In contrast, for stiff ring chains, the distribution of  $N_a$  exhibit a peak at  $N_a \approx 20$  across all densities, whereas the distribution of  $N_p$  shows two distinct peaks, one at  $N_p = 0$  and another at  $N_p \approx 20$ . In addition, the latter peak broadens as the density  $\rho$  increases. This observation implies that, when focusing on passive threading of stiff ring chains, they can be categorized into two different types: those having large loops facilitate threading and those lacking such structures. The latter rings are regarded as exhibiting more compact characteristic rather than those of the former.

## Conclusion

In summary, we employed PH analysis to characterize threading from MD simulations of the KG model for ring polymers. Specifically, we focused on the threading structure as influenced by the density  $\rho$  and chain stiffness  $\varepsilon_\theta$ , while maintaining the chain length of  $N = 400$ . Our analyses consists of three components: First, we examined the zero-th Betti number  $\beta_0(\alpha)$  to quantify the number of connected components formed by COMs of the polymers. This analysis demonstrates that numerous small clusters of COMs persist for flexible ring chains even at high densities, whereas a percolated network of COMs develops for stiff ring chains as the density increases. Second, we calculated the first Betti numbers,  $\beta_1(\alpha)$  and  $\tilde{\beta}_1(\alpha)$ , from  $\text{PD}(j \rightarrow i)$  to characterize the threading structure between pairs of ring chains. It is shown that stiff ring chains exhibit large-scale loops that facilitate threading as the density  $\rho$  increases. Furthermore, we also computed the active and passive threading numbers,  $N_a$  and  $N_p$ . As both  $\varepsilon_\theta$  and  $\rho$  increase, their averages become larger, indicating greater generations of threading, accompanied by the asymmetric behavior of the distributions of  $N_a$  and  $N_p$ . Finally, we introduced the threshold value  $l_{\text{th}}$  to emphasize long-lived threading structures in the calculations of  $N_a$  and  $N_p$ . This analysis reveals that the distributions of  $N_a$  and  $N_p$  converges to zero for flexible ring chains as the density increases. In contract, for stiff ring

chains, the distribution of  $N_p$  bifurcates into two distinct peaks, indicating heterogeneous threading structure characterized by rings with large-scale loops that facilitate threading and those that have compact ring characteristic. This heterogeneous threading structure observed in stiff ring chains serves as the underlying mechanism for topological glasses, which exhibit heterogeneous rearrangement dynamics of COMs analogous to those of glass-forming liquids.

## Acknowledgement

This work was supported by JSPS KAKENHI Grant-in-Aid Grant Nos. JP24H01719, JP22H04542, JP22K03550, JP23K27313, and JP23H02622. We also acknowledge the Fugaku Supercomputing Project (Nos. JPMXP1020230325 and JPMXP1020230327) and the Data-Driven Material Research Project (No. JPMXP1122714694) from the Ministry of Education, Culture, Sports, Science, and Technology and to Maruho Collaborative Project for Theoretical Pharmaceutics. The numerical calculations were performed at Research Center for Computational Science, Okazaki Research Facilities, National Institutes of Natural Sciences (Project: 24-IMS-C051). DM thanks the Royal Society for support through a University Research Fellowship and the European Research Council (ERC) under the European Union’s Horizon 2020 research and innovation program (grant agreement No 947918, TAP).

## References

- (1) Cates, M.; Deutsch, J. Conjectures on the Statistics of Ring Polymers. *J. Phys. France* **1986**, *47*, 2121–2128.
- (2) Müller, M.; Wittmer, J. P.; Cates, M. E. Topological Effects in Ring Polymers: A Computer Simulation Study. *Phys. Rev. E* **1996**, *53*, 5063–5074.
- (3) Grosberg, A. Y.; Nechaev, S. K.; Shakhnovich, E. I. The Role of Topological Constraints in the Kinetics of Collapse of Macromolecules. *J. Phys. France* **1988**, *49*, 2095–2100.

- (4) Sakaue, T. Ring Polymers in Melts and Solutions: Scaling and Crossover. *Phys. Rev. Lett.* **2011**, *106*, 167802.
- (5) Suzuki, J.; Takano, A.; Deguchi, T.; Matsushita, Y. Dimension of Ring Polymers in Bulk Studied by Monte-Carlo Simulation and Self-Consistent Theory. *J. Chem. Phys.* **2009**, *131*, 144902.
- (6) Tsolou, G.; Stratikis, N.; Baig, C.; Stephanou, P. S.; Mavrantzas, V. G. Melt Structure and Dynamics of Unentangled Polyethylene Rings: Rouse Theory, Atomistic Molecular Dynamics Simulation, and Comparison with the Linear Analogues. *Macromolecules* **2010**, *43*, 10692–10713.
- (7) Halverson, J. D.; Lee, W. B.; Grest, G. S.; Grosberg, A. Y.; Kremer, K. Molecular Dynamics Simulation Study of Nonconcatenated Ring Polymers in a Melt. I. Statics. *J. Chem. Phys.* **2011**, *134*, 204904.
- (8) Halverson, J. D.; Lee, W. B.; Grest, G. S.; Grosberg, A. Y.; Kremer, K. Molecular Dynamics Simulation Study of Nonconcatenated Ring Polymers in a Melt. II. Dynamics. *J. Chem. Phys.* **2011**, *134*, 204905.
- (9) Halverson, J. D.; Grest, G. S.; Grosberg, A. Y.; Kremer, K. Rheology of Ring Polymer Melts: From Linear Contaminants to Ring-Linear Blends. *Phys. Rev. Lett.* **2012**, *108*, 038301.
- (10) Bernabei, M.; Bacova, P.; Moreno, A. J.; Narros, A.; Likos, C. N. Fluids of Semiflexible Ring Polymers: Effective Potentials and Clustering. *Soft Matter* **2013**, *9*, 1287–1300.
- (11) Pasquino, R. et al. Viscosity of Ring Polymer Melts. *ACS Macro Lett.* **2013**, *2*, 874–878.
- (12) Brás, A. R.; Gooßen, S.; Krutyeva, M.; Radulescu, A.; Farago, B.; Allgaier, J.; Pyckhout-Hintzen, W.; Wischniewski, A.; Richter, D. Compact Structure and Non-Gaussian Dynamics of Ring Polymer Melts. *Soft Matter* **2014**, *10*, 3649–3655.

- (13) Slimani, M. Z.; Bacova, P.; Bernabei, M.; Narros, A.; Likos, C. N.; Moreno, A. J. Cluster Glasses of Semiflexible Ring Polymers. *ACS Macro Lett.* **2014**, *3*, 611–616.
- (14) Ge, T.; Panyukov, S.; Rubinstein, M. Self-Similar Conformations and Dynamics in Entangled Melts and Solutions of Nonconcatenated Ring Polymers. *Macromolecules* **2016**, *49*, 708–722.
- (15) Tsalikis, D. G.; Koukoulas, T.; Mavrantzas, V. G.; Pasquino, R.; Vlassopoulos, D.; Pyckhout-Hintzen, W.; Wischniewski, A.; Monkenbusch, M.; Richter, D. Microscopic Structure, Conformation, and Dynamics of Ring and Linear Poly(Ethylene Oxide) Melts from Detailed Atomistic Molecular Dynamics Simulations: Dependence on Chain Length and Direct Comparison with Experimental Data. *Macromolecules* **2017**, *50*, 2565–2584.
- (16) Iwamoto, T.; Doi, Y.; Kinoshita, K.; Takano, A.; Takahashi, Y.; Kim, E.; Kim, T.-H.; Takata, S.-i.; Nagao, M.; Matsushita, Y. Conformations of Ring Polystyrenes in Semidilute Solutions and in Linear Polymer Matrices Studied by SANS. *Macromolecules* **2018**, *51*, 6836–6847.
- (17) Mei, B.; Dell, Z. E.; Schweizer, K. S. Microscopic Theory of Long-Time Center-of-Mass Self-Diffusion and Anomalous Transport in Ring Polymer Liquids. *Macromolecules* **2020**, *53*, 10431–10445.
- (18) Jeong, S. H.; Cho, S.; Roh, E. J.; Ha, T. Y.; Kim, J. M.; Baig, C. Intrinsic Surface Characteristics and Dynamic Mechanisms of Ring Polymers in Solution and Melt under Shear Flow. *Macromolecules* **2020**, *53*, 10051–10060.
- (19) Kruteva, M.; Allgaier, J.; Monkenbusch, M.; Porcar, L.; Richter, D. Self-Similar Polymer Ring Conformations Based on Elementary Loops: A Direct Observation by SANS. *ACS Macro Lett.* **2020**, *9*, 507–511.

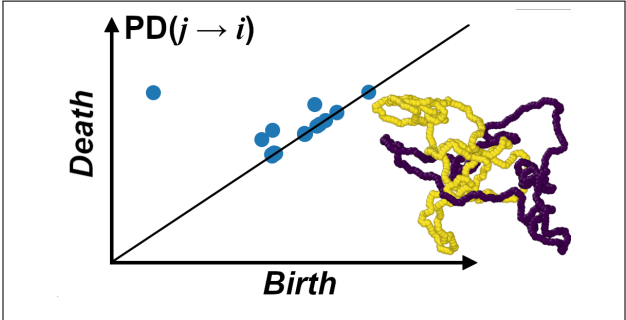


- (20) Mei, B.; Dell, Z. E.; Schweizer, K. S. Theory of Transient Localization, Activated Dynamics, and a Macromolecular Glass Transition in Ring Polymer Liquids. *ACS Macro Lett.* **2021**, *10*, 1229–1235.
- (21) Goto, S.; Kim, K.; Matubayasi, N. Effects of Chain Length on Rouse Modes and Non-Gaussianity in Linear and Ring Polymer Melts. *J. Chem. Phys.* **2021**, *155*, 124901.
- (22) Smrek, J.; Chubak, I.; Likos, C. N.; Kremer, K. Active Topological Glass. *Nat. Commun.* **2020**, *11*, 26.
- (23) Staño, R.; Likos, C. N.; Smrek, J. To Thread or Not to Thread? Effective Potentials and Threading Interactions between Asymmetric Ring Polymers. *Soft Matter* **2022**, *19*, 17–30.
- (24) Chubak, I.; Pachong, S. M.; Kremer, K.; Likos, C. N.; Smrek, J. Active Topological Glass Confined within a Spherical Cavity. *Macromolecules* **2022**, *55*, 956–964.
- (25) Roy, P. K.; Chaudhuri, P.; Vemparala, S. Effect of Ring Stiffness and Ambient Pressure on the Dynamical Slowdown in Ring Polymers. *Soft Matter* **2022**, *18*, 2959–2967.
- (26) Cai, X.; Liang, C.; Liu, H.; Zhang, G. Conformation and Structure of Ring Polymers in Semidilute Solutions: A Molecular Dynamics Simulation Study. *Polymer* **2022**, *253*, 124953.
- (27) Tu, M. Q.; Davydovich, O.; Mei, B.; Singh, P. K.; Grest, G. S.; Schweizer, K. S.; O’Connor, T. C.; Schroeder, C. M. Unexpected Slow Relaxation Dynamics in Pure Ring Polymers Arise from Intermolecular Interactions. *ACS Polym. Au* **2023**, *xxxx*, 307–317.
- (28) Kruteva, M.; Allgaier, J.; Richter, D. Topology Matters: Conformation and Microscopic Dynamics of Ring Polymers. *Macromolecules* **2023**, acs.macromol.3c00560.

- (29) Mei, B.; Grest, G. S.; Liu, S.; O'Connor, T. C.; Schweizer, K. S. Unified Understanding of the Impact of Semiflexibility, Concentration, and Molecular Weight on Macromolecular-Scale Ring Diffusion. *Proc. Natl. Acad. Sci. U.S.A.* **2024**, *121*, e2403964121.
- (30) Lo, W.-C.; Turner, M. S. The Topological Glass in Ring Polymers. *EPL* **2013**, *102*, 58005.
- (31) Michieletto, D.; Turner, M. S. A Topologically Driven Glass in Ring Polymers. *Proc. Natl. Acad. Sci. U.S.A.* **2016**, *113*, 5195–5200.
- (32) Michieletto, D.; Marenduzzo, D.; Orlandini, E.; Turner, M. Ring Polymers: Threadings, Knot Electrophoresis and Topological Glasses. *Polymers* **2017**, *9*, 349.
- (33) Sakaue, T. Topological Free Volume and Quasi-Glassy Dynamics in the Melt of Ring Polymers. *Soft Matter* **2018**, *14*, 7507–7515.
- (34) Smrek, J.; Grosberg, A. Y. Minimal Surfaces on Unconcatenated Polymer Rings in Melt. *ACS Macro Lett.* **2016**, *5*, 750–754.
- (35) Smrek, J.; Kremer, K.; Rosa, A. Threading of Unconcatenated Ring Polymers at High Concentrations: Double-Folded vs Time-Equilibrated Structures. *ACS Macro Lett.* **2019**, *8*, 155–160.
- (36) Tsalikis, D. G.; Mavrantzas, V. G. Threading of Ring Poly(Ethylene Oxide) Molecules by Linear Chains in the Melt. *ACS Macro Lett.* **2014**, *3*, 763–766.
- (37) Tsalikis, D. G.; Mavrantzas, V. G.; Vlassopoulos, D. Analysis of Slow Modes in Ring Polymers: Threading of Rings Controls Long-Time Relaxation. *ACS Macro Lett.* **2016**, *5*, 755–760.
- (38) Landuzzi, F.; Nakamura, T.; Michieletto, D.; Sakaue, T. Persistence Homology of Entangled Rings. *Phys. Rev. Research* **2020**, *2*, 033529.

- (39) Edelsbrunner, H.; Letscher, D.; Zomorodian, A. Topological Persistence and Simplification. Proceedings 41st Annual Symposium on Foundations of Computer Science. 2000; pp 454–463.
- (40) Edelsbrunner, H.; Harer, J. *Computational Topology: An Introduction*; American Mathematical Society: Providence, R.I, 2010.
- (41) Hiraoka, Y.; Nakamura, T.; Hirata, A.; Escolar, E. G.; Matsue, K.; Nishiura, Y. Hierarchical Structures of Amorphous Solids Characterized by Persistent Homology. *Proc. Natl. Acad. Sci. U.S.A.* **2016**, *113*, 7035–7040.
- (42) Kremer, K.; Grest, G. S. Dynamics of Entangled Linear Polymer Melts: A Molecular-dynamics Simulation. *J. Chem. Phys.* **1990**, *92*, 5057–5086.
- (43) Kratky, O.; Porod, G. Röntgenuntersuchung gelöster Fadenmoleküle. *Recueil des Travaux Chimiques des Pays-Bas* **1949**, *68*, 1106–1122.
- (44) Goto, S.; Kim, K.; Matubayasi, N. Unraveling the Glass-like Dynamic Heterogeneity in Ring Polymer Melts: From Semiflexible to Stiff Chain. *ACS Polym. Au* **2023**, *3*, 437–446.
- (45) Plimpton, S. Fast Parallel Algorithms for Short-Range Molecular Dynamics. *J. Comput. Phys.* **1995**, *117*, 1–19.
- (46) Obayashi, I.; Nakamura, T.; Hiraoka, Y. Persistent Homology Analysis for Materials Research and Persistent Homology Software: HomCloud. *J. Phys. Soc. Jpn.* **2022**, *91*, 091013.

# TOC Graphic



# Supporting Information:

## Persistent Homology Reveals the Role of Stiffness in Forming Topological Glasses in Dense Solutions of Ring Polymers

Shota Goto,<sup>†</sup> Takenobu Nakamura,<sup>‡</sup> Davide Michieletto,<sup>¶,§</sup> Kang Kim,<sup>\*,†</sup> and Nobuyuki Matubayasi<sup>\*,†</sup>

<sup>†</sup>*Division of Chemical Engineering, Department of Materials Engineering Science, Graduate School of Engineering Science, Osaka University, Toyonaka, Osaka 560-8531, Japan*

<sup>‡</sup>*National Institute of Advanced Industrial Science and Technology (AIST), 1-1-1 Umezono, Tsukuba, Ibaraki 305-8568, Japan*

<sup>¶</sup>*School of Physics and Astronomy, University of Edinburgh, Peter Guthrie Tait Road, Edinburgh, EH9 3FD, UK*

<sup>§</sup>*MRC Human Genetics Unit, Institute of Genetics and Cancer, University of Edinburgh, Edinburgh, EH4 2XU, UK*

E-mail: kk@cheng.es.osaka-u.ac.jp; nobuyuki@cheng.es.osaka-u.ac.jp

### Radius of gyration

For flexible ring polymers with the chain stiffness  $\varepsilon_\theta = 0$  in semidilute solutions, molecular dynamics (MD) simulations using the Kremer–Grest (KG) model reveal that the mean square

radius of gyration  $\langle R_g^2 \rangle$  as a function of density  $\rho$  follows the scaling behavior of  $\langle R_g^2 \rangle \sim \rho^{-0.59}$ .<sup>S1</sup> More specifically, using the mean square radius of gyration in the dilute limit, denoted as  $\langle R_g^{\circ 2} \rangle$ , and the overlap density  $3N/(4\pi\langle R_g^{\circ 2} \rangle^{3/2})$ , the scaling relation

$$\frac{\langle R_g^2 \rangle}{\langle R_g^{\circ 2} \rangle} = \left[ 1 + a \left( \frac{\rho}{\rho^*} \right) \right]^b, \quad (1)$$

was proposed. Here,  $a = 0.45$  and  $b = -0.59$  were the fitting parameters.

Figure S1 shows the chain stiffness  $\varepsilon_\theta$  dependence of the relationship between  $\langle R_g^2 \rangle / \langle R_g^{\circ 2} \rangle$  and  $\rho / \rho^*$  from our MD simulations. Note that  $\langle R_g^{\circ 2} \rangle$  was calculated at  $\rho = 0.001$ . The results reveal that  $\langle R_g^2 \rangle$  decreases with increasing density  $\rho$  and exhibits significant deviation from the scaling of Eq. (1) when chain stiffness  $\varepsilon_\theta$  is large, particularly noticeable for  $\rho / \rho^* > 1$ . This deviation from Eq. (1) implies that the influence of density  $\rho$  on chain conformation varies depending on the chain stiffness  $\varepsilon_\theta$ .

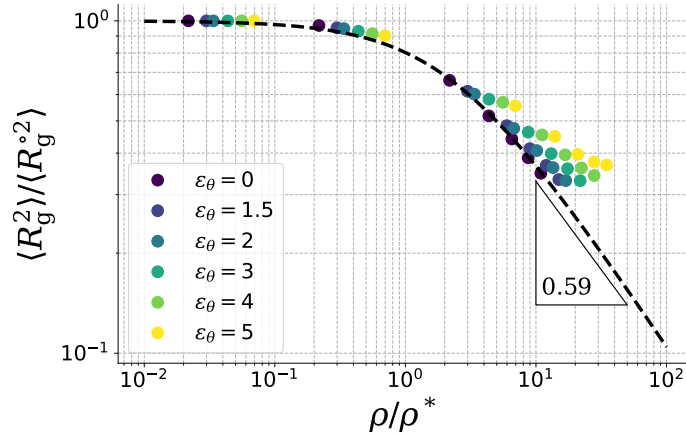


Figure S1: density  $\rho$  scaled by the overlap density  $\rho^*$  dependence of mean square radius of gyration  $\langle R_g^2 \rangle$  scaled by its dilute limit value  $\langle R_g^{\circ 2} \rangle$ .

## Radial distribution function of center of mass

We calculated the radial distribution function,  $g(r)$ , for center of mass (COM) of ring chains. The results are illustrated in Fig. S2. As demonstrated in Fig. S2,  $g(r)$  exhibits finite values

at the length scale  $r < \sqrt{\langle R_g^2 \rangle}$ , indicating significant interpenetration between the ring chains. For flexible ring polymers with  $\varepsilon_\theta = 0$ ,  $g(r)$  broadens with increasing density  $\rho$ , suggesting that the chains become less spatially separated from one another. In addition, for stiff ring polymers with  $\varepsilon_\theta = 5$ , the degree of interpenetration becomes more pronounced as the density  $\rho$  increases. This observation is attributed to the larger mean square radius of gyration,  $\langle R_g^2 \rangle$ , compared to that of flexible ring chains with  $\varepsilon_\theta = 0$  at the same  $\rho$  for dense systems (see Fig. S1). An analogous observation with respect to the chain stiffness and density dependence of  $g(r)$  for ring polymers was reported in a previous study.<sup>S2</sup>

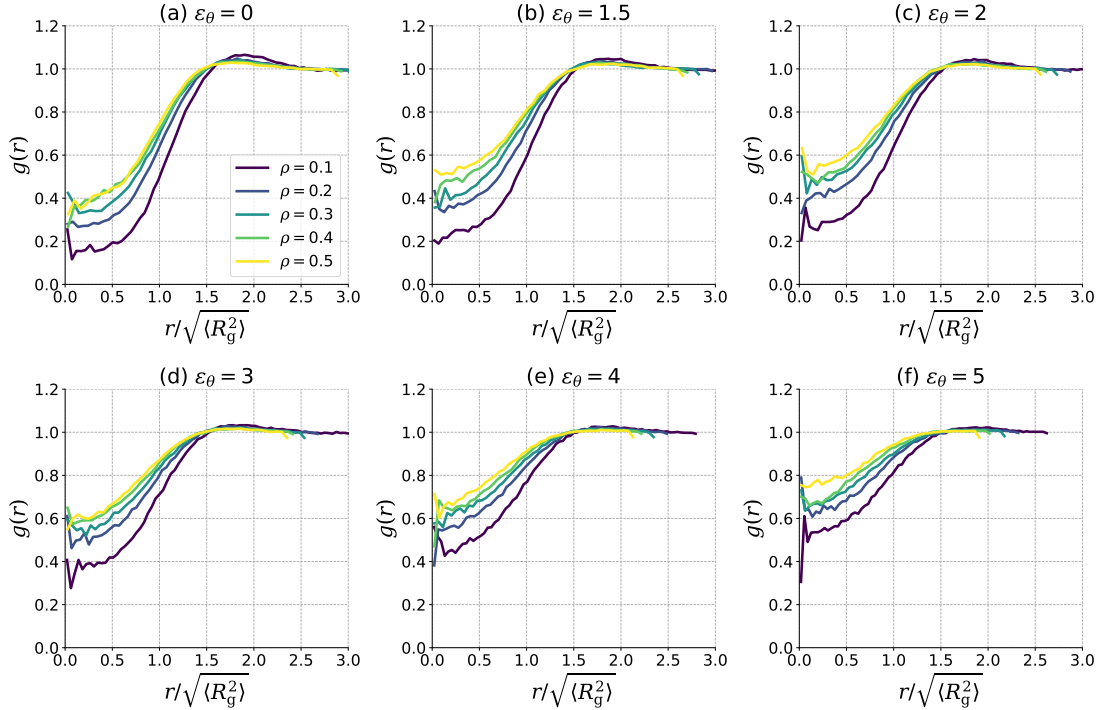


Figure S2: Radial distribution function  $g(r)$  for COM of ring polymers as a function of the scaled distance  $r/\sqrt{\langle R_g^2 \rangle}$  at  $\varepsilon_\theta = 0$  (a),  $\varepsilon_\theta = 1.5$  (b),  $\varepsilon_\theta = 2$  (c),  $\varepsilon_\theta = 3$  (d),  $\varepsilon_\theta = 4$  (e), and  $\varepsilon_\theta = 5$  (f).

## Virtual bond number

As shown in Figs. S1 and S2, the influence of density  $\rho$  on  $\langle R_g^2 \rangle$  and  $g(r)$  significantly varies with chain stiffness  $\varepsilon_\theta$ . To characterize the connectivity between COMs by varying  $\rho$  and  $\varepsilon_\theta$ , we introduced a virtual bond between ring polymers  $i$  and  $j$ . Specifically, if the distance between the COMs of polymers  $i$  and  $j$ , denoted as  $r_{ij}$ , satisfies

$$r_{ij} \leq \sqrt{\langle R_g^2 \rangle}, \quad (2)$$

the two polymer chains are considered to be virtually bonded.<sup>S3</sup> The number of virtual bonds is denoted as  $Z_b$ . The average number of virtual bonds can be expressed by

$$\langle Z_b \rangle = \int_0^{\sqrt{\langle R_g^2 \rangle}} 4\pi r^2 \left( \frac{\rho}{N} \right) g(r) dr. \quad (3)$$

Note that the threshold of the virtual bond is less than the contact distance,  $2\sqrt{\langle R_g^2 \rangle}$ , to emphasize the overlapping between COMs.

Figure S3 shows  $\langle Z_b \rangle$  as a function of density  $\rho$  by varying the chain stiffness  $\varepsilon_\theta$ . The  $\langle Z_b \rangle$  is an increasing function of  $\rho$ . As  $\varepsilon_\theta$  increases, the slope becomes steeper, indicating a greater dependence on  $\rho$ . In contrast, for flexible ring chains with  $\varepsilon_\theta = 0$ ,  $g(r/\sqrt{\langle R_g^2 \rangle})$  was found to saturate with increasing  $\rho$ , as demonstrated in the previous study.<sup>S1</sup> Similarly,  $\langle Z_b \rangle$  is also expected to approach saturation towards a finite value. This distinction in the density  $\rho$  dependence on the average number of virtual bonds  $\langle Z_b \rangle$  implies a significant difference in intermolecular interaction between ring polymers as the chain stiffness  $\varepsilon_\theta$  varies.



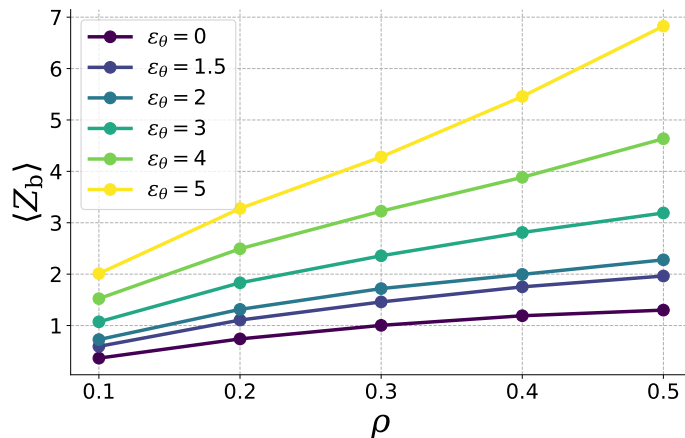


Figure S3: Density  $\rho$  dependence of the average number of virtual bonds,  $\langle Z_b \rangle$  by varying the chain stiffness  $\epsilon_\theta$ .

## Persistent diagram

Figures S4, S5, S6, and S7 present the probability density distributions of  $\text{PD}(i)$ ,  $\text{PD}(i \cup j)$ , and  $\text{PD}(j \rightarrow i)$  at combinations of  $(\epsilon_\theta, \rho) = (1.5, 0.1)$ ,  $(1.5, 0.5)$ ,  $(5, 0.1)$ , and  $(5, 0.5)$ , respectively. The general shape of  $\text{PD}(i)$  remains consistent regardless of variations in density  $\rho$  or chain hardness  $\epsilon_\theta$ . The area with the highest frequency appears close to the diagonal with a prominent vertical distribution at  $b \approx 0.22$ . The distribution along the diagonal line represents loops that are formed and quickly disappear. These short-lived loops, characterized by small values of life  $l$ , are typically regarded as noise because they do not significantly contribute to threading structures. In contrast, the distribution along  $b \approx 0.22$  is interpreted as loops generated by the inherent stiffness of the polymer chain backbone. Specifically, this value corresponds to the characteristic loop size related to the average bond length,  $l_b = 0.965 \approx 2\sqrt{0.22}$  of the KG model. The loops observed in the intermediate region, between the diagonal line and  $b \approx 0.22$ , are thought to be associated with secondary structures,<sup>S4</sup> such as the folding or compact configurations of ring polymers. These loops arise from internal conformational changes, bringing different parts of the polymer chain closer

together, forming transient or quasi-stable folded structures. Unlike short-lived loops near the diagonal line, these intermediate loops contribute to the overall topological complexity of the system.

In the  $\text{PD}(i \cup j)$ , the distribution along the diagonal is more extended compared to that of  $\text{PD}(i)$ . In addition, the intermediate distribution exhibits a more elongated shape. This is attributed to the creation of new loops caused by the contact between pairs of ring chains. These newly formed loops arise from the threading of ring chains, leading to an increase in the complexity of the structures, characterized by longer life  $l$ , due to the interaction between different chains. The distribution  $\text{PD}(j \rightarrow i)$ , representing the difference between  $\text{PD}(i)$  and  $\text{PD}(i \cup j)$ , does not exhibit significant changes compared to the shape of  $\text{PD}(i)$ . This indicates that the loops of one ring polymer are significantly influenced by the threading interaction with other ring polymers. A detailed discussion regarding the chain stiffness  $\varepsilon_\theta$  and density  $\rho$  is provided in the main text, where the analysis of the zero-th and first Betti numbers offers further insights.

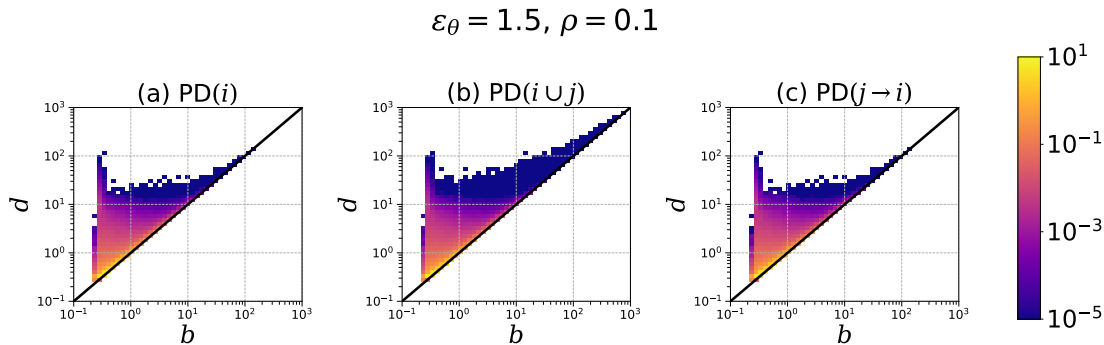


Figure S4: Persistent diagrams,  $\text{PD}(i)$  (a),  $\text{PD}(i \cup j)$ , and  $\text{PD}(i \rightarrow j)$ , with  $\varepsilon = 1.5$  and  $\rho = 0.1$ .

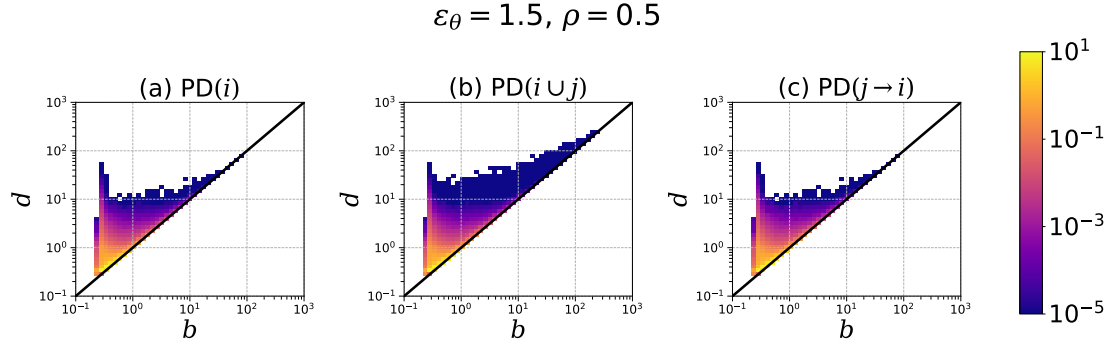


Figure S5: Persistent diagrams, PD( $i$ ) (a), PD( $i \cup j$ ), and PD( $i \rightarrow j$ ), with  $\varepsilon = 1.5$  and  $\rho = 0.5$ .

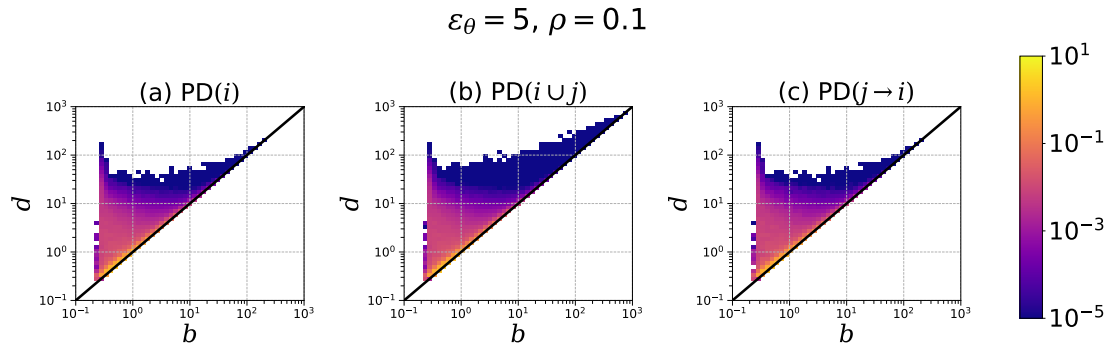


Figure S6: Persistent diagrams, PD( $i$ ) (a), PD( $i \cup j$ ), and PD( $i \rightarrow j$ ), with  $\varepsilon = 5$  and  $\rho = 0.1$ .

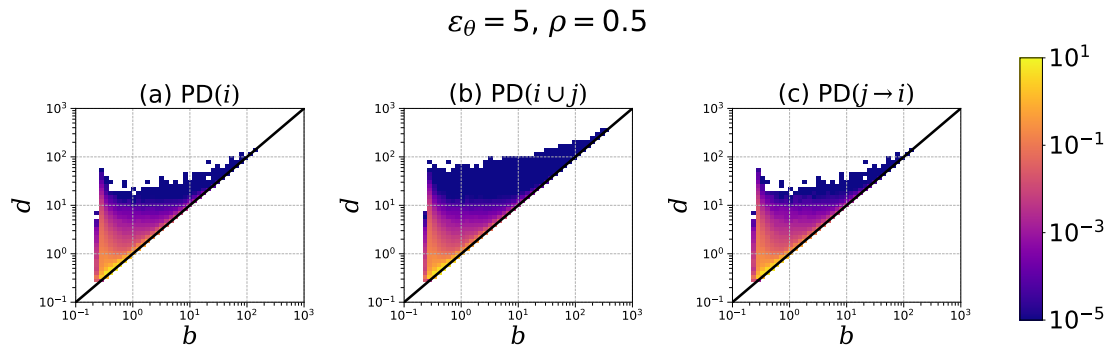


Figure S7: Persistent diagrams, PD( $i$ ) (a), PD( $i \cup j$ ), and PD( $i \rightarrow j$ ), with  $\varepsilon = 5$  and  $\rho = 0.5$ .

# First Betti number

Figure S8 shows  $\beta_1(\alpha)$  and  $\tilde{\beta}_1(\alpha)$  for varying  $\rho$  and  $\varepsilon_\theta$ . As the density increases, this peak sharpens, with its position shifting to smaller  $\alpha$ , signifying the formation of smaller loops. However, the discrepancy in  $\beta_1(\alpha)$  and  $\tilde{\beta}_1(\alpha)$  between flexible and stiff rings becomes more pronounced with increasing density  $\rho$ . This observation aligns with the fact that the density  $\rho$  dependence of the mean square radius of gyration  $\langle R_g^2 \rangle$  exceeds the expected scaling behavior of  $\langle R_g^2 \rangle \sim \rho^{-0.59}$  for stiff rings as  $\rho$  increases (see Fig. S1).

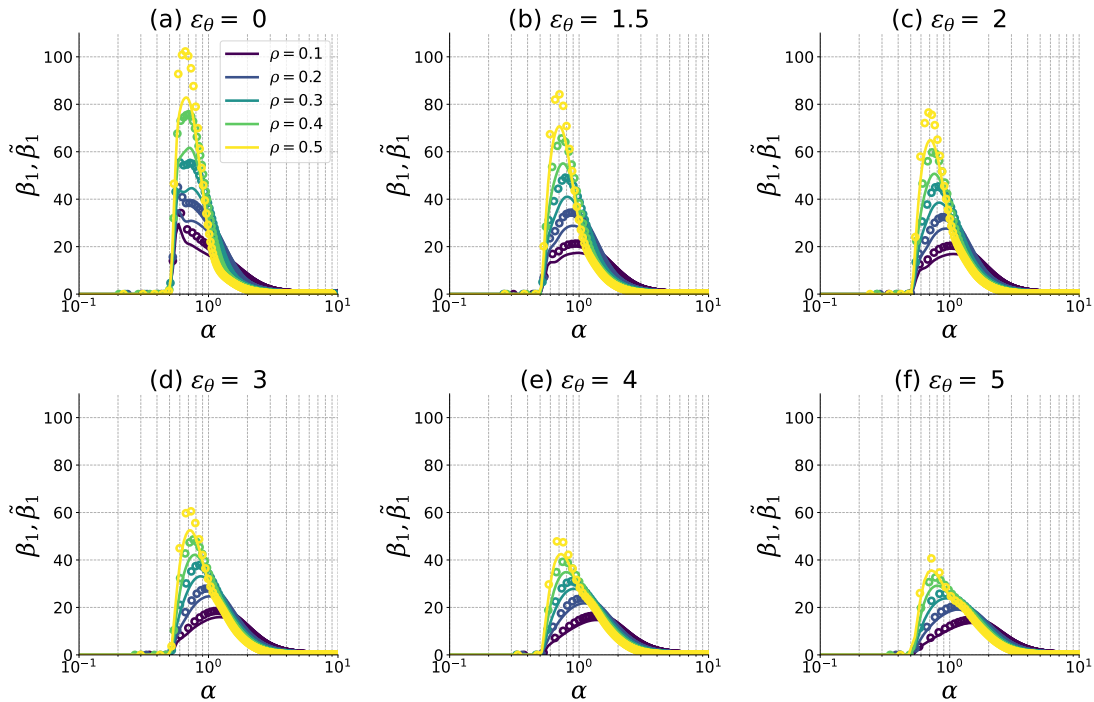


Figure S8: Density  $\rho$  dependence of  $\beta_1(\alpha)$  (points) and  $\tilde{\beta}_1(\alpha)$  (solid curves) by varying the bending energy  $\varepsilon_\theta = 0$  (a),  $\varepsilon_\theta = 1.5$  (b),  $\varepsilon_\theta = 2$  (c),  $\varepsilon_\theta = 3$  (d),  $\varepsilon_\theta = 4$  (e), and  $\varepsilon_\theta = 5$  (f).

## References

- (S1) Cai, X.; Liang, C.; Liu, H.; Zhang, G. Conformation and Structure of Ring Polymers in Semidilute Solutions: A Molecular Dynamics Simulation Study. *Polymer* **2022**, *253*, 124953.

- (S2) Bernabei, M.; Bacova, P.; Moreno, A. J.; Narros, A.; Likos, C. N. Fluids of Semiflexible Ring Polymers: Effective Potentials and Clustering. *Soft Matter* **2013**, *9*, 1287–1300.
- (S3) Goto, S.; Kim, K.; Matubayasi, N. Unraveling the Glass-like Dynamic Heterogeneity in Ring Polymer Melts: From Semiflexible to Stiff Chain. *ACS Polym. Au* **2023**, *3*, 437–446.
- (S4) Hiraoka, Y.; Nakamura, T.; Hirata, A.; Escolar, E. G.; Matsue, K.; Nishiura, Y. Hierarchical Structures of Amorphous Solids Characterized by Persistent Homology. *Proc. Natl. Acad. Sci. U.S.A.* **2016**, *113*, 7035–7040.